FLOW AND HEAT TRANSFER CHARACTERISTICS OF A SELF ENTRAINING EJECTOR CONICAL DIFFUSER WITH AND WITHOUT SLOT GUIDANCE

Singh L., Singh S. N.* and Sinha S. S.
*Author for correspondence
Department of Applied Mechanics,
Indian Institute of Technology Delhi,
New Delhi 110016,
India,
*E-mail: sns@am.iitd.ac.in

ABSTRACT

Self entraining diffusers are mechanical devices which are used to entrain ambient (cold) air to mix with the exhaust (hot) gases. These devices are commonly used at the rear of the gas turbine engines with the aim of cooling the exhaust gases without putting back pressure on the engine and in the process suppress the IR signatures. The performance of self entraining diffuser is critical when employed in helicopters and ships since the hot exhaust gases coming out of the gas turbines engines can be detected by infrared sensing missiles. The current study numerically investigates two conical self entraining diffusers, one with no slot guidance (conventional) and other with slot guidance while keeping all other geometrical parameters such as slot area, diffuser area ratio, diffuser angle, length of the diffuser, standoff distance, etc same. The simulation is carried out at fixed Reynolds number. The performance of the two self entraining diffuser is compared in terms of local and overall temperature drop, mass entrainment, pressure recovery and mixing.

We find that the local temperature drop for slot guided diffuser is significantly high near the diffuser wall. The mass entrainment at each slot is also higher for guided slot. For slot guided diffuser, an additional peak in the velocity magnitude is seen due to the presence of guided slot which allow the primary flow in the diffuser to retain axial momentum over a larger distance. The overall temperature drop is higher for slot guided self entraining diffuser with improved pressure recovery.

INTRODUCTION

The advancements in the gas-turbine(GT) technology has pushed the limits of power to weight ratio of the engine and thus leading to maximum temperature limits obtainable [1]. This has resulted in the elevated exhaust temperature. Gas turbines have been used to power many applications which also include airborne vehicles, ships, etc. Higher exhaust temperature values results into prominent infrared signatures, which makes the engine and the vehicle easily detectable by heat seeking missiles. The development in the field of infrared sensing mechanism like advancement in detector array technology and processors has led to the further increase in the effectiveness of the IR seeking missiles [2], [3] which in turn demands demands improvement in the IR Signature Suppression (IRSS) techniques. There are several techniques which could improve the IRSS [4] and one such method is the use of an Ejector-Diffuser assembly [5] which can be integrated on the exhaust side of a GT engine.

Ejector diffuser is a passive mechanical device. They are designed for achieving temperature drop of the exhaust gases with no back pressure. There are three main component of ejector diffuser (i) nozzle, (ii) mixing tube and (iii) self entraining diffuser

NOMENCLATURE

D_{nz}	[m]	Diameter of nozzle
D_{mx}	[m]	Diameter of mixing tube
L_{mx}	[m]	Length of the mixing tube
D_{mx}	[m]	Diameter of the mixing tube
AR_{mx}	[-]	Area ration of mixing tube inlet to nozzle exit
L_{sd}	[m]	Length of standoff distance
L_{df}	[m]	Length of the diffuser
AR_{df}	[-]	Area ratio of diffuser exit to diffuser inlet
L_{tp}	[m]	Length of the tail pipe
D_{pl}	[m]	Diameter of the plenum
α	[-]	Diffuser half angle
U_{in}	[m/s]	Nozzle exit velocity
T_{in}	[K]	Nozzle exit temperature
r	[m]	Cylinderical radial direction
z	[m]	Cylinderical axis direction

Subscripts

nz	nozzle
mx	mixing tube
sd	standoff distance
df	diffuser
tp	tail pipe
pl	plenum
in	nozzle exit

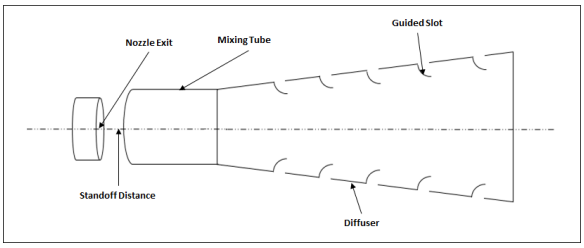

Figure 1. Schematic of Ejector Diffuser

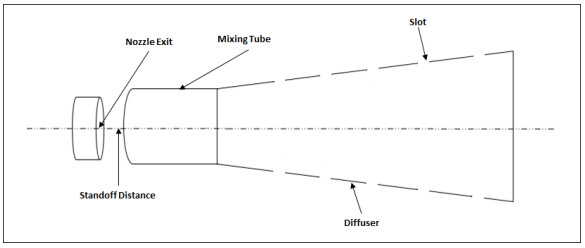

Figure 2. Schematic of Ejector Diffuser without guided slots

as shown in the figure 1.

The important performance parameters for an ejector diffuser are the mass entrainment ratio, drop in exhaust temperature and its uniformity, static pressure recovery and mixing of exhaust gases with atmospheric air within the mixing tube and diffuser. However, these performance indicators are strong function of geometrical and dynamical parameters such as length, area ratio, diffuser angle, slot size, number of slots, slot inclination, shape of slots, standoff distance, etc. Sen [6] has found that standoff distance between $2D_{nz}$ to $3D_{nz}$ offers maximum entrainment for the conical stepped ejector diffuser. Chen and Birk [7] has found that oblong shaped ejector diffuser offers higher mixing at 30° swirl when compared with conical shaped ejector diffuser. Singh et al [8] studied stepped square shaped ejector diffuser and concluded that the performance of the ejector diffuser becomes independent when Reynolds Number is greater than 10^4 and another study by Singh et al [9] found that with increase in number of slots the mass entrainment does not improve but there is slight improvement in static pressure recovery. The higher mass entrainment with zero back pressure along with significant temperature drop are the most important design criteria. However an independent investigation on the slot geometric configuration has not been studied yet. Further we know that entrainment occurs through slots and thus modifying slot shapes can result in improved performance. The present investigation aims to study the influence of guiding the flow at the slop which also influences the flow within the diffuser (as shown in figure 1). Performance of this ejector diffuser assembly (Figure 1) is evaluated by comparing simulation results with those obtained without guided slot as shown in figure 2.

Geometrical Details

All the geometrical details for the two cases have been kept same expect the presence of guided slot in one case. To obtain the shape of guided curve, we have chosen a circular arc as shown in figure 3 . The circular arc is generated from two coordinates and a conditions that the trailing edge of the guided slot is parallel to diffuser axis. These two coordinates corresponds to (i) endpoint of the diffuser wall (marked as circle in the figure 3) and (ii) point of intersection of two imaginary straight lines perpendicular to each other (point marked as circle in figure 3).

MATHEMATICAL FORMULATION

Under this section, we provide details about our computational domain, boundary conditions, governing equations and solver settings.

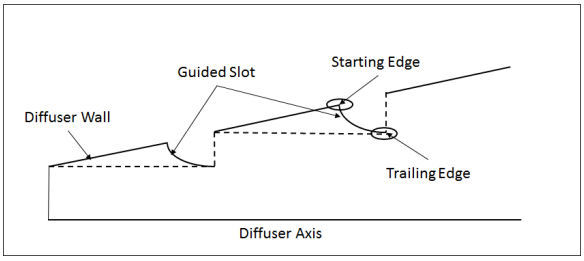

Figure 3. Geometric details of curved guided slots

Computational Domain and Boundary Conditions

The current study has been performed on a two dimensional axi-symmetrical computational domain. The computational domain and the boundary conditions are shown in figure 4. All the

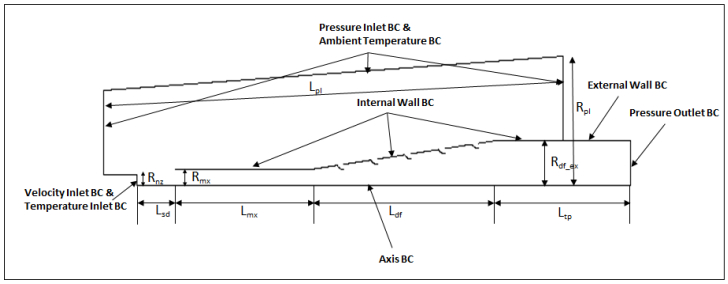

Figure 4. Computational domain and boundary conditions

dimensions of the computation domain are defined in terms of nozzle diameter D_{nz}. All important dimensions are listed in table 1.

Table 1. Location within the Mixing Tube

L_{sd}	$2.25D_{nz}$	Distance between mixing tube inlet and nozzle exit
AR_{mx}	2.25	Area ratio of mixing tube inlet to nozzle exit
L_{mx}	$8D_{nz}$	Length of the mixing tube
D_i	$1.5D_{nz}$	Diffuser inlet diameter
L_{df}	$11D_{nz}$	Length of the diffuser
AR_{df}	8	Area ratio of diffuser exit to diffuser inlet
L_{tp}	$32D_{nz}$	Length of the tail pipe
D_{pl}	5-8D_{nz}	Diameter of Plenum
2α	14.2°	Diffuser angle

At the nozzle exit, the flow is expected to be a plug flow and hence normal component of the velocity to the nozzle exit is assigned in the form of velocity inlet boundary condition (BC) at 60 m/s with fixed inlet temperature of 700°K. The wall of the mixing tube and diffuser are assigned viscous wall BC. The three sides of the plenum are set at ambient conditions hence pressure inlet BC with zero gauge pressure and ambient temperature con-

dition at 300°K are imposed at these boundaries. At the exit of the tail pipe, flow is released at atmospheric conditions so pressure outlet BC as zero gauge pressure is set as appropriate BCs.

The meshing of the computational domain is achieved through quadrilateral cell elements for both the cases and thereby a structured mesh is obtained for analysis. The quality of the mesh cells is monitored through aspect ratio and angle formed by the sides of a cell. The maximum aspect ratio for the mesh cells is maintained at less than 100 while the worst cell has an angle more than 45°. The $y+ < 5$ is maintained near the walls to capture large velocity gradients.

Governing equations

The governing equations for steady, 2-D axisymmetric flow are Reynolds averaged continuity (1) and momentum (2) equations.

$$\nabla.(\rho\vec{v}) = 0 \tag{1}$$

$$\nabla.(\rho\vec{v}\vec{v}) = -\nabla p + \nabla.(\bar{\bar{\tau}}) \tag{2}$$

where ρ is density of the fluid, $\vec{v}$ and p represent Reynolds-averaged velocity and pressure respectively. The symbol $\bar{\bar{\tau}}$ represent total stress tensor where

$$\bar{\bar{\tau}} = \mu^{eff}(\nabla\vec{v} + \nabla\vec{v}^T) \tag{3}$$

The symbol μ^{eff} is the sum of molecular viscosity (μ) and turbulent viscosity (μ_t)

$$\mu^{eff} = (\mu + \mu_t) \tag{4}$$

The governing equation for conservation of energy (5) is solved to get temperature distribution in the domain. In equation (5), k_{eff} is the effective conductivity and represent the sum of material thermal conductivity and turbulent thermal conductivity.

$$\rho c_p(\vec{v}.\nabla)T = k_{eff}\nabla^2 T \tag{5}$$

Two equation turbulence models are considered to close the RANS set of equations (1-5),

Earlier studies [9], [6] and [10] on ejector diffuser are conducted by different two-equation turbulence models such as standard k-ε [11], Realizable k-ε [12] and SST k-ω [13]. We employ SST k-ω turbulence model for simulating the two cases. We chose SST k-ω turbulence model after conducting a systematic comparison of various turbulence models in capturing velocity profile in the ejector diffuser and plotted against the experimental data of Sen[6].

Equations refkinematic eddy viscosity to 13 are additional set of equations in SST k-ω model for closure of RANS equations. Equation (6) is the relationship between eddy (turbulent) viscosity and k and ω variables . Equation (7) and (8) are governing equations for k and ω, and equations (9) to (13) give the closure coefficients and auxilary relations for the SST k-ω turbulence models. The time derivative term is dropped in (7), (8) as the flow is statistically steady.

$$\nu_T = \frac{a_1 k}{max(a_1\omega, SF_2)} \tag{6}$$

$$\nabla.(\vec{v}k) = P_k - \beta^* k\omega + \nabla.(\nu + \sigma_k\nu_T)\nabla k \tag{7}$$

$$\nabla.(\vec{v}\omega) = \alpha S^2 - \beta\omega^2 + \nabla.[(\nu + \sigma_\omega\nu_T)\nabla\omega] + 2(1-F_1)\sigma_{\omega 2}\frac{1}{\omega}\nabla k\nabla\omega \tag{8}$$

Closure coefficients and Auxilary Relations

$$F_2 = tanh\left[\left[\left(\frac{2\sqrt{k}}{\beta^*\omega y}, \frac{500\nu}{y^2\omega}\right)\right]^2\right] \tag{9}$$

$$P_k = min\left(\tau_{ij}\nabla\vec{v}, 10\beta^* k\omega\right) \tag{10}$$

$$F_1 = tanh\left\{\left\{min\left[max\left(\frac{\sqrt{k}}{\beta^*\omega y}, \frac{500\nu}{y^2\omega}\right), \frac{4\sigma_{\omega 2}k}{CD_{k\omega}y^2}\right]\right\}^4\right\} \tag{11}$$

$$CD_{k\omega} = max\left(2\rho\sigma_{\omega 2}\frac{1}{\omega}\nabla k\nabla\omega, 10^{-10}\right) \tag{12}$$

$$\phi = \phi_1 F_1 + \phi_2(1-F_1) \tag{13}$$

$$a_1 = \frac{5}{9}, a_2 = 0.44$$

$$\beta_1 = \frac{3}{40}, \beta_2 = 0.0828$$

$$\beta^* = \frac{9}{100}$$

$$\sigma_{k1} = 0.085, \sigma_{k2} = 1$$

$$\sigma_{\omega 1} = 0.5, \sigma_{\omega 2} = 0.856$$

Discretization scheme

Second order upwind scheme has been adopted to discretize momentum, turbulent kinetic energy and specific dissipation rate (ω) equations. The pressure velocity coupling is achieved using SIMPLE scheme. The absolute convergence criteria for continuity, momentum, k and ω and T are kept at 10^{-6}.

Grid convergence studies

The results are obtained after performing a detailed grid independence study where simulation are conducted for different grid sizes. The geometrical dimension are retained as our original case. The Reynolds Number is 2×10^5. Four different mesh sizes as shown in table 2 are selected for mesh independence study. Figure 5 gives the velocity magnitude variation after slot

Table 2. Grid sizes for mesh independence study

Mesh Type	Cell count
Grid 1	100000
Grid 2	260000
Grid 3	300000
Grid 4	400000

1. It is seen that there is no change in velocity profile for Grid 3 and Grid 4 and hence Grid 3 is used for the present study.

RESULTS AND DISCUSSION

Our simulations have been performed out on a conical self entraining ejector diffuser with and without slot guidance. We will refer the two cases as A and B (table 3) The results are presented in two parts. In Part I, mass entrainment in the two cases are compared. In Part II, influence of entrainment in temperature profile is studied.

Table 3. Simulation cases for the current study

Case A	Slot guided conical self entraining diffuser
Case B	Without slot guided conical self entraining diffuser

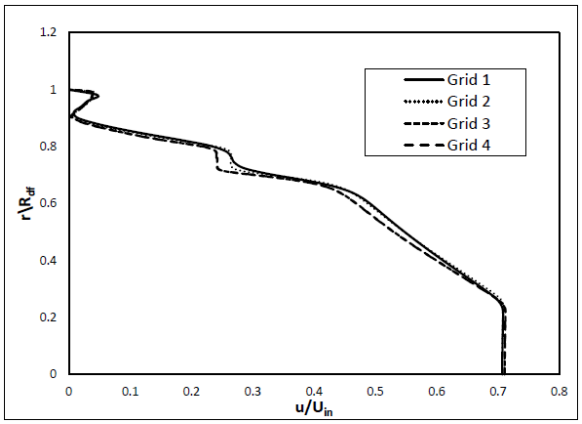

Figure 5. Velocity profile comparison mesh size 100000, 260000, 300000 and 400000.

Mass Entrainment

Mass entrainment in an ejector diffuser happens through the openings provided along the length of the diffuser and also through standoff distance. The amount of entrained mass is directly influenced by velocity magnitude of the primary fluid. A higher velocity is associated with lower pressure in the core of the diffuser, which in turn enables better entrainment. In figure

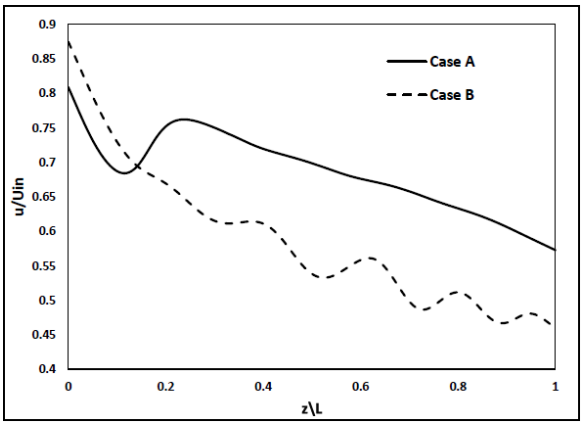

Figure 6. Centerline velocity magnitude comparison

6 we show the variation of axial velocity along the diffuser axis observed in cases A and B. In this perspective, velocity magnitude is plotted at the axis for Case A and Case B as shown in the figure 6. We observe that downstream of slot 1, the axial velocity is significantly larger in Case A than Case B. Accordingly the static pressure (gauge) is expected to be lower in Case A than Case B. Indeed this is confirmed by figure 7(highlighted by the box) which shows lower static pressure in Case A.

The overall effect of higher core velocity (lower static pressure) is expected to enhanced mass entrainment through peripheral slots. In figure 8 we plot cumulative entrained mass ratio (CER) along the diffuser axis. CER is defined as

$$CER = \sum m_{je}/m_{in}$$

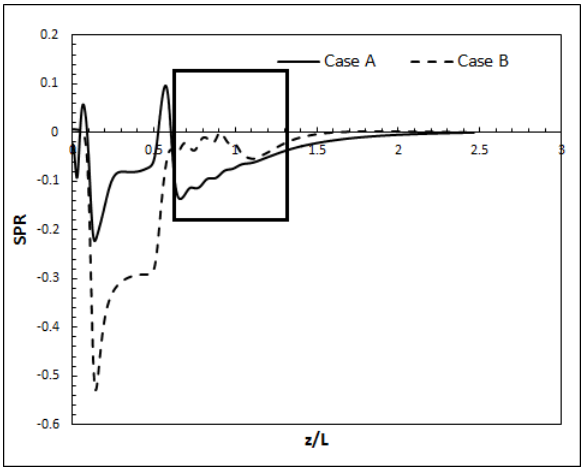

Figure 7. Static pressure at the axis of ejector diffuser

where m_{je} is the sum of mass flow rates through standoff distance, through the j^{th} slot and all the slots upstream of the j^{th} slot and m_{in} is nozzle exit mass flow rate. We observed that CER

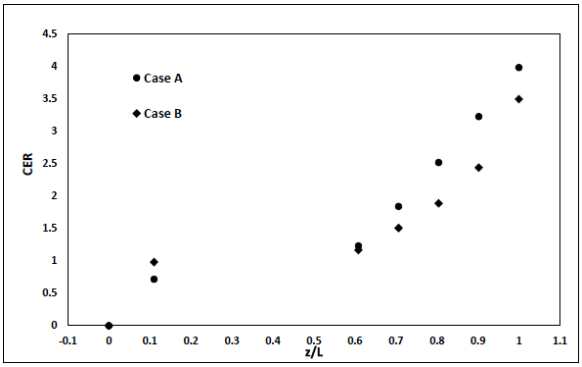

Figure 8. Cumulative mass entrainment through openings along the ejector diffuser

in Case A is consistency higher than Case B throughout the diffuser. On one to one comparison at slots, the % increase in mass flow rate ranges between 5.5% to 33.33% while overall Case A has14% more mass entrainment.Thus based on these observation we conclude that an ejector diffuser with guided slots shows much improved performance as compared to an ejector diffuser without guided slot in terms of entrained mass.

To better understand the flow physics in the two cases we present streamline pattern in Case A and Case B. Figure 9 represent the streamline for Case A(top figure) and Case B. We observe that in both cases primary flow enters into the diffuser and it starts to expand along the wall of the diffuser. However, due to the presence of slot guidance curve (Slot 1) in Case A, the primary flow is forced toward the central core region and enabling it to maintain higher axial velocity in the core.

Influence of Mass entrainment on Temperature Profiles

The temperature of the jet exiting the nozzle is fixed at 700°K and the ambient conditions are fixed at 300°K. Figure 10 shows the temperature contour plot in two simulation cases. We ob-

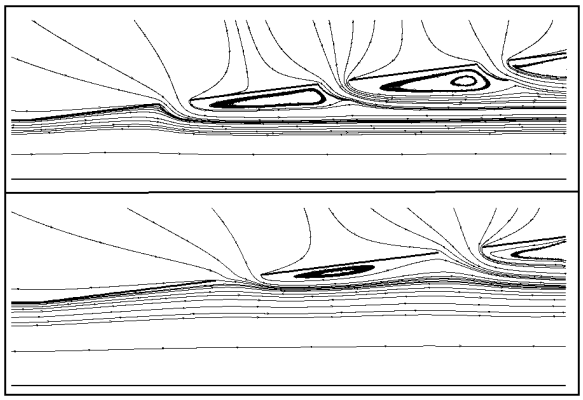

Figure 9. Streamlines near the diffuser wall. Case A: Top image, Case B: Bottom image

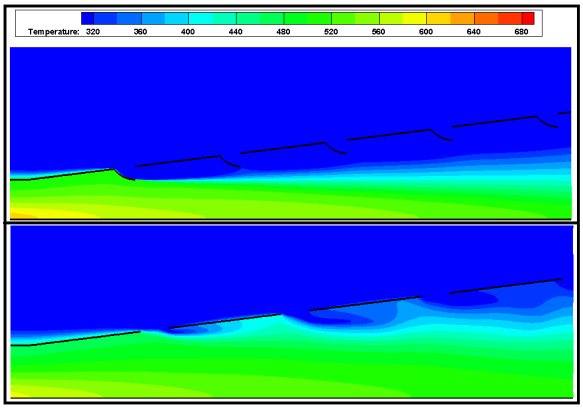

Figure 10. Variation of temperature in the computational domain. Case A: Top image, Case B: Bottom image

serve that in Case A bigger annulus cold zone is formed near the diffuser wall at all axial locations. Further the temperature observed in the near wall region is lower in Case A compared to Case B.

This distribution of temperature can be explained by investigating velocity profile (since heat transfer is dominated by convection). Velocity profile downstream of slot 1 for both the cases is shown in figure 11. For case B the velocity profile has only one small peak close to the wall and afterwards velocity increase monotonically as we move towards the diffuser axis. However for Case A, there are two peaks close to the diffuser wall itself ($1 < r/R_{df} < 0/7$). This also becomes more clearer from figure 9. It can be seen that the recirculation pockets in Case A are bigger than Case B. Also these pockets tends to grow in size for Case A as we move along the diffuser wall. Based on these observations it is plausible to suggest that convecting action of these recirculation zones allow for development of a layer of colder zone near the diffuser wall in Case A then in Case B.

To estimate the overall temperature drop in the two cases, temperature profiles for Case A and Case B are plotted downstream of slot 5 (last slot) as shown in the figure 12. We can see that for large annulus region between diffuser wall to 0.3 distance, Case A has smaller values of temperature compared to Case B. An area

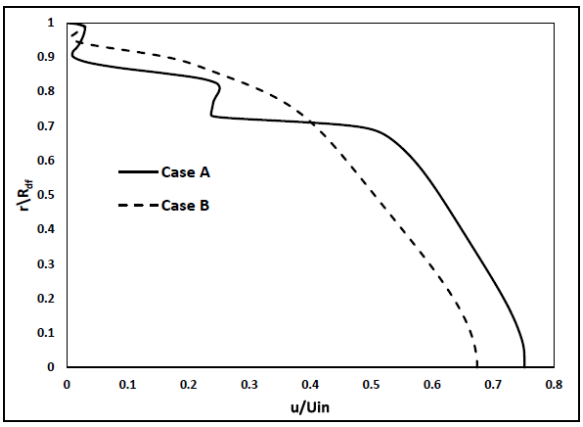

Figure 11. Velocity magnitude after slot 1

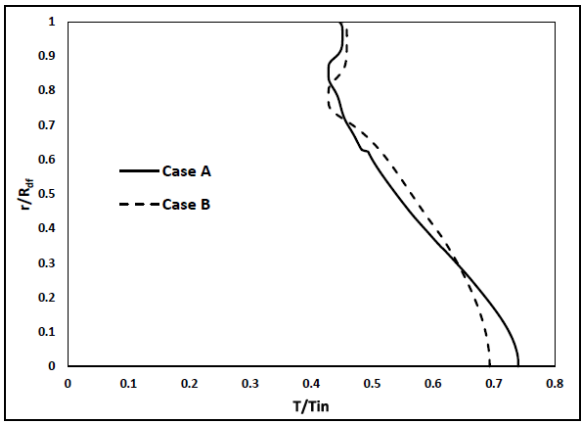

Figure 12. Temperature profile after slot 5

weighted temperature at this location for Case A is 342.75°K and for Case B is 356.57°K which reflects 15°K more temperature drop from Case A.

CONCLUSION

Numerical simulations have been conducted for two dimensional axisymmetric conical self entraining ejector diffuser with and without guided slot. All geometrical and dynamical parameters have been kept the same for both the cases except one has guided slot (Case A) and other has no guided slot (Case B). The shape selected for the guided slot is a circular arc whose trailing edge is parallel to the diffuser axis. The following are the important conclusions of this study:

1. Higher mass entrainment is recorded for slot guided ejector diffuser with an overall increase of 14%.
2. Larger cold zone annulus is formed near the diffuser wall in slot guided ejector diffuser.
3. Guided slots allow the primary flow in the diffuser to retain axial momentum over a larger distance.
4. The overall temperature drop to 342.75°K is within the acceptable limits.

It is concluded that improved performance can be achieved with guided slot ejector diffuser compared to the ejector diffuser without guided slot.

REFERENCES

[1] Pilavachi, P.A., Power generation with gas turbine systems and combined heat and power. *Applied Thermal Engineering*, Vol. 20, No. 15, 2000, pp.1421-1429.

[2] Paterson, J., Overview of low observable technology and its effects on combat aircraft survivability. *Journal of Aircraft*, Vol. 36, No. 2, 1999, pp.380-388.

[3] Rao, G.A. and Mahulikar, S.P., New criterion for aircraft susceptibility to infrared guided missiles. *Aerospace science and technology*, Vol. 9, No. 8, 2005, pp.701-712.
Gebbie, H.A., Harding, W.R., Hilsum, C., Pryce, A.W. and Roberts, V., March. Atmospheric Transmission in the 1 to 14 *mu* Region. *In Proceedings of the Royal Society of London A: Mathematical, Physical and Engineering Sciences* Vol. 206, No. 1084, 1951, pp. 87-107. The Royal Society.

[4] Mahulikar, S.P., Prasad, S. and Potnuru, S.K., Infrared signature suppression of helicopter engine duct based on" Conceal and Camouflage". *Journal of Propulsion and Power*, Vol. 24, No. 3, 2008, pp.613-618.

[5] Birk, A.M. and Davis, W.R., Suppressing the infrared signatures of marine gas turbines. *TRANS. ASME J. ENG. GAS TURBINES POWER*, Vol. 111 No. 1, 1989, pp.123-129.
Singh, P., Singh, S. N., and Seshadri, V., Effect of number of slots and overlap on the performance of Non-circular Ejector Air Diffuser, *Proceedings of the 43rd AIAA Fluid Dynamics Conference*, 2013, pp. 2729

[6] Sen, S., Studies on Flow Characteristics of a Stepped Conical Diffuser with Passive Suction, *PHD Thesis, Department of Applied Mechanics, IIT Delhi*,2008

[7] Chen, Q. and Birk, A.M., Experimental and CFD study of an exhaust ejector with round entraining diffuser. *In ASME Turbo Expo 2007: Power for Land, Sea, and Air* 2007, January. (pp. 27-35). American Society of Mechanical Engineers.

[8] Singh, P., Singh, S. and Seshadri, V., Experimental Investigations on Non-Circular Ejector Air Diffusers. *In 39th AIAA Fluid Dynamics Conference*, 2009, pp. 4213.

[9] Singh, P. and Singh, S.N., Effect of number of slots and overlap on the performance of Non-circular Ejector Air Diffuser. *In 32nd AIAA Applied Aerodynamics Conference* 2014, pp. 2837.

[10] Chen, Q., Performance of air-air ejectors with multi-ring entraining diffusers. 2008.

[11] Launder, B.E. and Spalding, D.B., The numerical computation of turbulent flows. *Computer methods in applied mechanics and engineering*, Vol 3, No 2, 1974, pp.269-289.

[12] Shih, T.H., Liou, W.W., Shabbir, A., Yang, Z. and Zhu, J., A new k-ε eddy viscosity model for high reynolds number turbulent flows. *Computers and Fluids*, Vol 24, No 3, 1995, pp.227-238.

[13] Menter, F.R., Two-equation eddy-viscosity turbulence models for engineering applications. *AIAA journal*, Vol 32, No 8, 1994, pp.1598-1605.